Laser induced fluorescence measurements of axial velocity, velocity shear, and parallel ion temperature profiles during the route to plasma turbulence in a linear magnetized plasma device

S. Chakraborty Thakur,[1,a)] K. Adriany,[1] J. J. Gosselin,[1] J. McKee,[2] E. E. Scime,[2] S. H. Sears,[3] and G. R. Tynan[1]

[1]*Center for Energy Research, University of California at San Diego, San Diego, California 92093-0417, USA*
[2]*Department of Physics and Astronomy, West Virginia University, Morgantown, West Virginia 26506, USA*
[3]*Department of Physics, University of Wisconsin at Madison, Madison, Wisconsin 53706, USA*

(Presented 8 June 2016; received 10 June 2016; accepted 24 June 2016; published online 2 August 2016)

We report experimental measurements of the axial plasma flow and the parallel ion temperature in a magnetized linear plasma device. We used laser induced fluorescence to measure Doppler resolved ion velocity distribution functions in argon plasma to obtain spatially resolved axial velocities and parallel ion temperatures. We also show changes in the parallel velocity profiles during the transition from resistive drift wave dominated plasma to a state of weak turbulence driven by multiple plasma instabilities. *Published by AIP Publishing.* [http://dx.doi.org/10.1063/1.4959275]

I. INTRODUCTION

Plasma flows in fusion devices are critically important for several reasons. The lifetime of plasma facing components in a fusion device is governed by material erosion, migration, and redeposition, and hence, accurate measurements of the scrape-off-layer (SOL) flows are necessary.[1,2] However, scarcity of multi-point measurements makes impurity studies in the SOL plasma flows difficult. Moreover, these flow measurements are generally made with Mach probes,[1] whose interpretation is subject to considerable debates.[3–5] Hence, here we used non-perturbative laser induced fluorescence (LIF) for Doppler resolved spectroscopic measurements of ion flows.[6]

Plasma flows in fusion devices are also the key to understand plasma turbulence. Simpler geometry and better diagnostics access allow detailed drift turbulence and shear flow studies in linear plasma devices.[7–10] Strong shear flows also give rise to velocity shear driven instabilities.[11] Toroidal rotation is beneficial for both MHD control and suppression of micro-instabilities. Intrinsic rotation,[12,13] driven by the residual turbulent stresses, is also of prime interest and linear plasma devices provide an ideal test bed to study intrinsic flows in a magnetic shear free regime.[14]

Previous studies[15] in the Controlled Shear Decorrelation eXperiment (CSDX) have demonstrated that with increasing magnetic field (**B**), density gradient driven drift wave fluctuations evolve from narrow-band coherent azimuthal modes to a state of weak turbulence characterized by broadened frequency and wave number spectra. Nonlinear energy transfer analyses[16] have shown that for $\mathbf{B} \sim 1000$ G, energy is transferred from the higher frequency ($f \sim 10$ kHz, $m = 3$ mode) turbulent fluctuations to a low frequency ($f < 1$ kHz, $m = 0$ mode) azimuthally symmetric shear flow, thus having characteristics of zonal flows. More recent experiments[17] on an upgraded CSDX (higher **B**, larger antenna with $m = 1$ helical source) have shown that a global transition occurs at a threshold magnetic field $\mathbf{B_{th}}$ (which depends on the source parameters). Below $\mathbf{B_{th}}$, the plasma is dominated by density gradient driven collisional drift wave instabilities. A new global equilibrium is found for $\mathbf{B} > \mathbf{B_{th}}$, with coexistence of three radially separated plasma instabilities: coherent high azimuthal mode number fluctuations in the central core; collisional drift waves in the density gradient region; and strong, turbulent, shear-driven instabilities at the edge. This new regime shows very rich plasma dynamics including intermittency, formation and propagation of blobs, formation of a radial internal transport barrier which explain the blue-core formation in helicon sources, inward particle flux against density gradients, spontaneous self-organized transport bifurcation, etc.[17–21] In this paper, we investigate the axial velocity and the velocity shear, and parallel ion temperatures in CSDX, which relate to both studies of plasma impurity entrainment[22] and generation of intrinsic flows.[14]

II. EXPERIMENTAL APPARATUS

The experiments were carried out in CSDX, a linear magnetized plasma device, 2.8 m long with 0.2 m diameter (see Fig. 1). Argon plasma is produced by a 13.56 MHz, 1.8 kW, $m = 1$ helicon antenna with diameter 0.15 m. CSDX is immersed in a magnetic field up to 2400 G. At the standard operating conditions (3.2 mTorr of neutral fill pressure at 25 SCCM of neutral argon flow), typical electron temperatures and plasma densities in CSDX, as measured by RF compensated cylindrical Langmuir probes, are $T_e \sim 3$ eV and $n \sim 10^{13}$ cm^{-3}, respectively. More details of the experimental device, the operating regimes, the plasma diagnostics, and typical radial profiles of the standard plasma parameters can be found

Note: Contributed paper, published as part of the Proceedings of the 21st Topical Conference on High-Temperature Plasma Diagnostics, Madison, Wisconsin, USA, June 2016.

a)Author to whom correspondence should be addressed. Electronic mail: saikat@ucsd.edu.

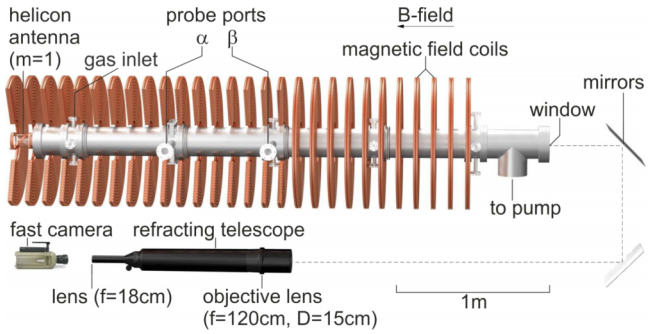

FIG. 1. The experimental device CSDX.

elsewhere.[17,18,23] Insulating end boundaries were used as they enhance turbulence levels in CSDX.[24,25] All data shown are obtained at the port named α in Fig. 1, ~75 cm downstream of the plasma source.

III. DIAGNOSTICS

For the three level LIF scheme used here, the laser light at 668.6138 nm is absorbed to induce a transition from the Ar-II metastable $3d^4F_{7/2}$ state to the $4p^4D_{5/2}$ state causing a photon to be re-emitted at 442.72 nm, through a transition to the $4s^4P_{3/2}$ state.[10] The magnetic field causes this transition to split into one group of six linearly polarized π transitions ($\boldsymbol{m} = 0$) and two orthogonal, circularly polarized groups of six σ transitions each ($\boldsymbol{m} = \pm 1$) due to Zeeman effect. We used a Toptica TA100 tunable diode laser (Fig. 2(a)) with a line width of ~1 MHz and a mode hop free range of up to 30 GHz. A beam splitter was used to redirect 8% of the beam into a Bristol Instruments 621-VIS wavemeter, to measure the wavelength with an accuracy of ±0.000 05 nm which corresponds to an instrumental error of ~±25 m/s. Another 8% of the beam is directed to an iodine cell. A quarter wavelength plate was used to choose only the $\boldsymbol{m} = 1$ circularly polarized σ branch, which consist of six Zeeman split lines.

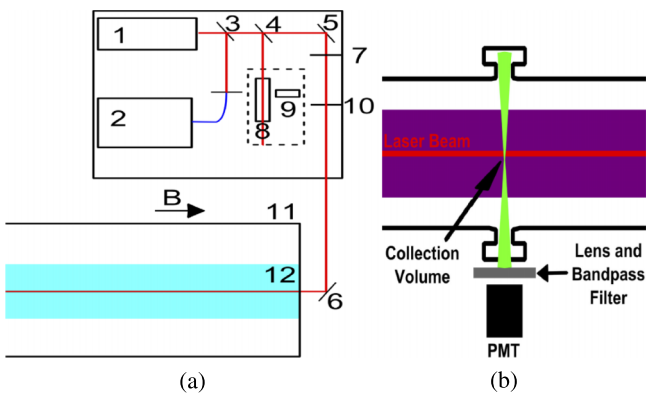

FIG. 2. Details of the LIF diagnostics: (a) the injection setup where 1 is the diode laser; 2 is the wavemeter; 3 and 4 are 8% beam splitters; 5 and 6 are turning mirrors; 7 is a quarter wave-plate, 8 is an iodine cell; 9 is a photo-multiplier tube; 10 is a mechanical chopper; 11 is the CSDX chamber; and 12 is the plasma column. The dotted lines represent a box to cover the iodine cell and photo-multiplier. (b) Collection setup.

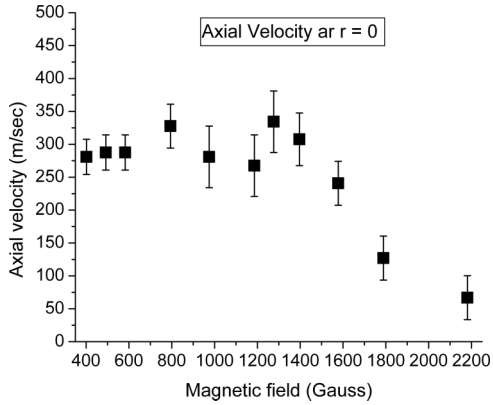

FIG. 3. Axial velocities measured at $r = 0$ cm, as **B** is varied.

Laser light centered at 668.6138 nm was injected parallel to the magnetic field through a window at the pump end of CSDX. The laser frequency was scanned over 10-20 GHz to capture the full ion velocity distribution function (IVDF). The emitted florescence was collected through a side port using a focusing optic and 1 nm width bandpass filter centered at 443 nm in front of a photo multiplier tube (PMT) (see Fig. 2(b)). The overlap of the focused collection optics and the laser beam forms a collection volume of ~3 mm^3, the spatial resolution of the measurements. Since this transition can also be collisionally excited by electron impact, phase synchronous detection was performed by modulating the beam intensity with a chopper at 1 kHz and a lock-in amplifier. The injection and the collection optics were moved in tandem to access multiple spatial locations to measure radial profiles.

For this argon ion transition, the Doppler and Zeeman broadening are the only two relevant line broadening mechanisms.[26] The relative magnitudes and the shifts of the Zeeman splitting of the lines can be calculated from quantum mechanical considerations.[27] Since the Zeeman splitting and Doppler broadening are of the same order, the data need to be fit with a convolution of six Doppler broadened Maxwellian functions (since we choose only the $m = 1$ circularly polarized σ branch). The measured intensity is fit to the following equation:

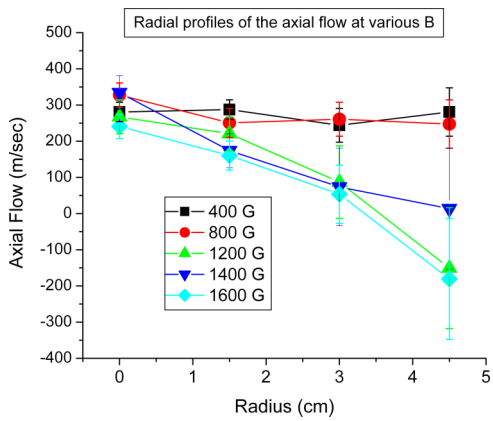

FIG. 4. Radial profiles of axial velocities below and above $\mathbf{B_{th}}$.

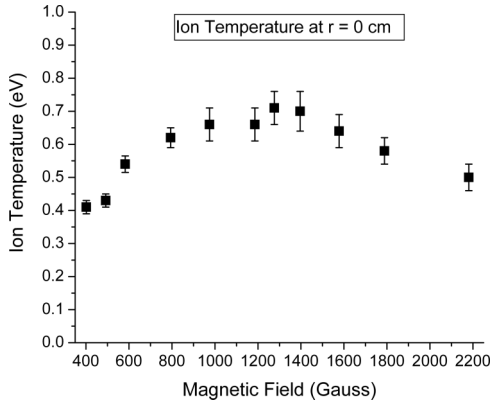

FIG. 5. Parallel ion temperatures at $r = 0$ cm, as **B** is varied.

$$I(\nu) = \sum_n I_n \exp(\kappa_\nu \frac{(\nu - \delta\nu - \nu_n)^2}{T_i}), \quad (1)$$

where I_n and ν_n represent the relative amplitudes and Zeeman shifts for each transition line, T_i is the ion temperature, the Doppler shift is given by $\delta\nu$, and κ_ν is a constant (0.092 495 eV/GHz^2). The best fit of Eq. (1) to the measured IVDF using a nonlinear least squares fitting routine gives the Doppler shift and the ion temperature.

IV. RESULTS AND DISCUSSIONS

The radial profiles of the axial flows and ion temperatures are measured for **B** = 400 G to **B** = 2200 G, to complement other studies of the transition at $\mathbf{B_{th}} \sim 1300$ G. In Fig. 3, we see that the axial velocity, measured at the center of the plasma device, remains almost constant with increasing **B** until $\mathbf{B} \sim \mathbf{B_{th}}$. For $\mathbf{B} > \mathbf{B_{th}}$, the core axial velocity decreases rapidly. Recent experiments show plasma detachment at the end for $\mathbf{B} > \mathbf{B_{th}}$ and this could be related to the drop of the axial velocities in this regime.

In Fig. 4, we show the radial profiles of the axial velocity, for **B** above and below the $\mathbf{B_{th}}$. We find that for low **B**, the flow profiles are almost flat with little to no radial shear in the axial velocities. However as we approach $\mathbf{B_{th}}$ and go beyond, we observe the development of a strong radial shear in the axial velocities. We are currently investigating if the energy from the parallel shear flow instability plays any role in the global transition at $\mathbf{B_{th}}$. Recent theoretical work has also shown[14] that in the absence of magnetic shear, as in CSDX, parallel velocity shear can lead to a new physical mechanism of driving intrinsic rotation via symmetry breaking and these preliminary results from CSDX agree with these arguments.

Fig. 5 shows that the parallel ion temperature, measured at the center of the device ($r = 0$ cm), increases with **B** (for $\mathbf{B} < \mathbf{B_{th}}$), reaches a maximum for $\mathbf{B} \sim \mathbf{B_{th}}$ and for $\mathbf{B} > \mathbf{B_{th}}$, the ion temperature drops. The edge ion temperature near the wall of the device is almost constant for all values of **B**. Hence this indicates increased ion temperature gradients (ITGs) near $\mathbf{B_{th}}$. Existence of multiple instabilities suggests multiple energy sources involved and the ion temperature gradient (ITG) driven instability might be relevant. In tokamaks, it has been seen that the nature of instabilities has a crucial role in deciding the direction of rotation for intrinsic rotation along the toroidal direction[12,13] and effects of parallel ITG on turbulence dynamics are being studied in CSDX.

In conclusion, we measured parallel flows, radial shear in the parallel flows, and parallel ion temperatures in CSDX. These studies complement our efforts in understanding the global transition from drift wave dominated plasmas to a multi-instability regime with several interesting characteristics.[17–21] The axial flow measurements have also resolved several earlier issues with impurity transport studies on CSDX[28] and the applicability of Mach probes.[22] We figured out the physical reasons for a systematic error in the interpretation of Mach probes. Comparison to LIF results helped us to introduce a correction term in the analysis of Mach probe data to fix the systematic error due to perturbative probe shadows in magnetized plasmas.[22]

[1]R. A. Pitts *et al.*, Plasma Phys. Controlled Fusion **47**, B303 (2005).
[2]G. F. Matthews, J. Nucl. Mater. **337-339**, 1 (2005).
[3]L. Oksuz, M. A. Khedr, and N. Hershkowitz, Phys. Plasmas **8**, 1729 (2001).
[4]I. H. Hutchinson, Phys. Plasmas **9**, 1832 (2002).
[5]K.-S. Chung, Plasma Sources Sci. Technol. **21**, 063001 (2012).
[6]G. D. Severn, D. A. Edrich, and R. McWilliams, Rev. Sci. Instrum. **69**, 10 (1998).
[7]G. R. Tynan, C. Holland, J. H. Yu, A. James, D. Nishijima, M. Shimada, and N. Taheri, Plasma Phys. Controlled Fusion **48**, S51 (2006).
[8]Y. Nagashima *et al.*, Phys. Plasmas **16**, 020706 (2009).
[9]T. Windisch, O. Grulke, and T. Klinger, J. Nucl. Mater. **390**, 395 (2009).
[10]T. A. Carter and J. E. Maggs, Phys. Plasmas **16**, 012304 (2009).
[11]E. Thomas, Jr., J. D. Jackson, E. A. Wallace, and G. Ganguli, Phys. Plasmas **10**, 1191 (2003).
[12]J. Rice *et al.*, Nucl. Fusion **44**, 379 (2004).
[13]B. LaBombard *et al.*, Phys. Plasmas **12**, 056111 (2005).
[14]J. C. Li, P. H. Diamond, X. Q. Xu, and G. R. Tynan, Phys. Plasmas **23**, 052311 (2016).
[15]M. J. Burin, G. R. Tynan, G. Y. Antar, N. A. Crocker, and C. Holland, Phys. Plasmas **12**, 052320 (2005).
[16]P. Manz, M. Xu, S. C. Thakur, and G. R. Tynan, Plasma Phys. Controlled Fusion **53**, 095001 (2011).
[17]S. C. Thakur, C. Brandt, L. Cui, J. J. Gosselin, A. D. Light, and G. R. Tynan, Plasma Sources Sci. Technol. **23**, 044006 (2014).
[18]A. D. Light, S. C. Thakur, C. Brandt, Y. Sechrest, G. R. Tynan, and T. Munsat, Phys. Plasmas **20**, 082120 (2013).
[19]S. C. Thakur, C. Brandt, L. Cui, J. J. Gosselin, and G. R. Tynan, IEEE Trans. Plasma Sci. **43**, 2754 (2015).
[20]L. Cui, G. R. Tynan, P. H. Diamond, S. C. Thakur, and C. Brandt, Phys. Plasmas **22**, 050704 (2015).
[21]L. Cui, A. Ashourvan, S. C. Thakur, R. Hong, P. H. Diamond, and G. R. Tynan, Phys. Plasmas **23**, 055704 (2016).
[22]J. J. Gosselin, S. C. Thakur, S. H. Sears, J. McKee, E. E. Scime, and G. R. Tynan, Phys. Plasmas **23**, 073519 (2016).
[23]S. C. Thakur, C. Brandt, A. Light, L. Cui, J. J. Gosselin, and G. R. Tynan, Rev. Sci. Instrum. **85**, 11E813 (2014).
[24]S. C. Thakur, M. Xu, P. Manz, N. Fedorczak, C. Holland, and G. R. Tynan, Phys. Plasmas **20**, 012304 (2013).
[25]D. A. D'Ippolito, D. A. Russell, J. R. Myra, S. C. Thakur, G. R. Tynan, and C. Holland, Phys. Plasmas **19**, 102301 (2012).
[26]R. F. Boivin, "Study of the different line broadening mechanisms for the laser induced fluorescence diagnostic of the HELIX and LEIA plasmas, PL-039, West Virginia University," Morgantown, WV, 2002.
[27]R. F. Boivin, "Zeeman splitting for LIF transitions and de-convolution technique to extract ion temperatures," PL-050, West Virginia University, Morgantown, WV, 2002.
[28]J. J. Gosselin, Ph.D. thesis, University of California at San Diego, 2016.